GEOCHEMISTRY

Intense overpressurization at basaltic open-conduit volcanoes as inferred by geochemical signals: The case of the Mt. Etna December 2018 eruption

Antonio Paonita[1]*, Marco Liuzzo[1], Giuseppe Salerno[2], Cinzia Federico[1], Piero Bonfanti[2], Antonio Caracausi[1], Giovanni Giuffrida[1], Alessandro La Spina[2], Tommaso Caltabiano[2], Sergio Gurrieri[1], Gaetano Giudice[2]

The balance between the amount of gas coexisting with mantle-derived magmas at depth and that emitted during intereruptive phases may play a key role in the eruptive potential of volcanoes. Taking the December 2018 eruption at Mt. Etna volcano as a case study, we discuss the geochemical data streams observed. The signals indicate a long-lasting prelude stage to eruption, starting in 2017 and involving magma-fluid accumulation in the deep (>7 km bsl) reservoir, followed by pressure buildup in the system at intermediate depth (5 to 2 km bsl), 6 to 7 months before the eruption. A brief preeruptive phase marks the pressurization at 2 to 3 km below the craters. By comparing the magma and fluid recharge at depth to the measured volcanic degassing from the plume, we provide evidence that Mt. Etna was in a state of extreme overpressurization in the weeks before the onset of the eruption.

INTRODUCTION

Injection of magma plus gas into magmatic chambers can be regarded as a main trigger of eruptive activity in volcanoes (*1*, *2*). The consequent buildup of the internal pressure controls the amount of magma leaving the chamber, the failure of wall rocks, and dike opening right up to the eruption (*3*). However, the extent of the pressure buildup depends closely on the capacity of the system to quickly dispose of the excess pressure (*4*) and, because magmatic gases are indisputably considered the driving force of the pressurization (*5*), the time-dependent balance between inputted gases at depth and volcanic outgassing on the surface becomes a critical parameter in determining the eruptive potential of a volcano. There are several pieces of evidence indicating that the amount of gas released by volcanoes is remarkably higher than that corresponding to the erupted magma volumes (*6*–*10*) or residing in shallow reservoirs. This proves that magmas are oversaturated with respect to the vapor phase at crustal depth long before the eruption and that the eruptive style is largely driven by the degassing of the unerupted magma (*11*–*13*). As an example, the flushing of mantle-derived CO_2, its accumulation at various levels in the plumbing system, and the extent of crystallization were suggested to be responsible for the intensity of explosive activity at Mt. Etna (*14*). The balance between the gas contained in mantle-derived magmas and the amount of gas emitted during quiescent or eruptive phases could represent a key factor in revealing the efficiency in gas percolation through the feeding system or the potential gas accumulation at depth. This, in turn, has marked consequences on the occurrence and style of eruptions. Wallace (*11*) observed that the excess of volatiles originating from the mantle-derived supply is approximately balanced during explosive eruptions. On these grounds, our ability to measure gas output from volcanoes by remote-sensing techniques (*15*–*20*) can be combined with recent developments in estimating deep recharges in magmatic systems (*21*–*23*), with the aim of assessing the general state of pressurization of a volcano and, ultimately, its eruptive potential.

Mt. Etna is an outstanding candidate to attempt this kind of estimation, thanks to the very frequent eruptive activity, the presence of well-developed monitoring networks designed to measure the degassing of the volcano (*24*–*26*), and the availability of suitable models to recognize and quantify the deep magma recharges (*23*). In particular, the so-called Christmas Eve eruption in December 2018 is an exemplary case where a sudden intrusive event, of very short duration but accompanied by intense degassing, seismicity, and ground deformation (*27*–*34*), suggests a substantial buildup of pressure inside the volcano. Here, we integrate data from the multiparametric geochemical monitoring of Mt. Etna to detect and track the magmatic processes leading to the December 2018 eruption from the deep recharge of magma to its migration and arrival at the surface. We show that the investigated signals, which include the geochemistry of peripheral gas vents, the diffuse flux of CO_2 from volcano flanks, and the output and composition of plume degassing, "see" different windows of depth in the feeding system, allowing us to follow the time-dependent process of magma ascent. Last, we combine the estimated magma recharge at depth with our measurements of volcanic degassing to highlight that Mt. Etna was extraordinarily overpressurized before the onset of the Christmas eruption.

RESULTS

Studied data and signals in this work were collected by continuous monitoring networks installed on Mt. Etna and by discrete samplings carried out at specific sites (Fig. 1 and Materials and Methods). The geochemical monitoring has detected signals of particular interest at the time of/during the "Christmas Eve eruption", both before the eruptive activity and syn- and posteruptive. In Fig. 2, we show the investigated parameters considered in this study between January 2017 and February 2019. Regarding the isotope ratio of He in the five monitored peripheral sites (Fig. 2A), it is notable that the signal began a long upward trend already in the first half of 2017,

[1]Istituto Nazionale di Geofisica e Vulcanologia - Sezione di Palermo, Via Ugo La Malfa 153, 90146 Palermo Italy. [2]Istituto Nazionale di Geofisica e Vulcanologia - Sezione di Catania, Piazza Roma 2, 95125 Catania Italy.
*Corresponding author. Email: antonio.paonita@ingv.it

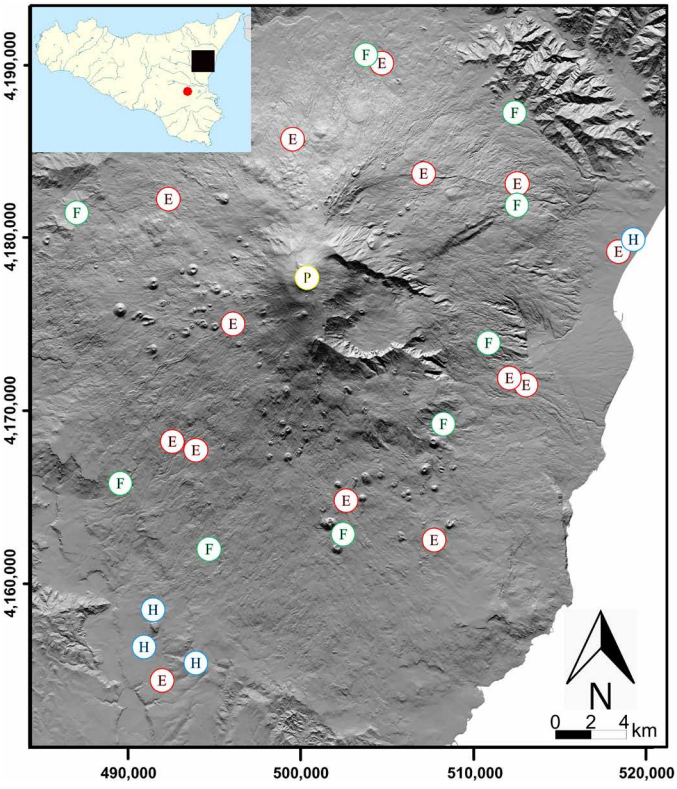

Fig. 1. Location of the measurement sites at Mt. Etna. The figure shows the permanent networks of INGV: CO_2 flux from soils EtnaGAS (E), SO_2 flux FLAME (F), and CO_2/SO_2 ratio EtnaPLUME (P). The location of sites selected for monitoring the $^3He/^4He$ ratio of peripheral gases is also shown (H). The inset indicates the location of Mt. Etna (black square) and the position of the furthest helium sampling site (red circle).

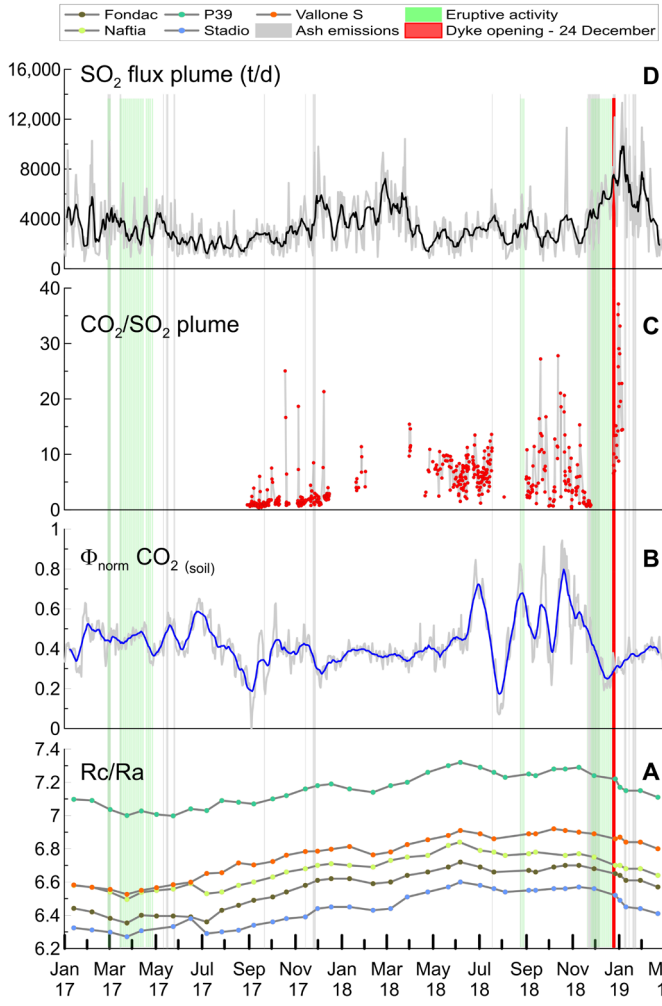

Fig. 2. Investigated geochemical signals in the period July 2017 to February 2019. From bottom to the top: (**A**) $^3He/^4He$ isotope ratio in peripheral gas vents (as R/Ra, see the main text); (**B**) Normalized curve of the total flows of CO_2 exhaling from the soils recorded by the EtnaGAS network (daily and running average on weekly basis as gray and blue lines, respectively); (**C**) CO_2/SO_2 ratio measured in the Etna plume; and (**D**) the daily and weekly bulk SO_2 flux measured in the volcanic plume (gray and black lines, respectively). The volcano activity of the studied period is also shown by distinguishing eruptive and ash emission events (green, gray headbands) and the eruptive phase of December 24 (red band).

although with a slight decrease between January and February 2018, culminating in June (see also fig. S1). A slight decrease of the $^3He/^4He$ ratio is then observed until the beginning of August 2018, followed by stable or slightly increasing values until November, and slightly decreasing but still high values until the sampling campaign of 27 December, a few days after the eruption onset. The two subsequent sampling campaigns on 2 and 10 January 2019 showed a significant drop in the $^3He/^4He$ ratio.

Figure 2B shows the diffuse flux of CO_2 from the volcano flanks, measured by the EtnaGAS network, after the appropriate normalizations described in Materials and Methods section. After the first 6 months of 2018, characterized by a stable signal at medium-low levels, it is evident that from June, the values increased markedly and remained high until the autumn of 2018. In detail, the values oscillated up and down over 4 cycles, with similar peak amplitude, namely, in June, August, September, and October. From the end of November 2018 until the beginning of the eruption, the values fell to very low levels, indicating very modest degassing from the flanks of the volcano edifice.

The bulk flux of SO_2 emitted by the Etnean plume and remotely measured via the flux automatic measurements (FLAME) network from July 2017 is shown in Fig. 2D. The signal showed changes at both temporal and magnitude scales, with values exceeding the typical degassing of Etna during quiescent conditions (*26*, *35*, *36*). These changes are consistent with eruptive activity and geophysical signals observed at Mt. Etna over the 26 months of our study. Overall, the SO_2 flux displayed two main waning-waxing phases featured by relevant gas emissions: (i) between September 2017 and March 2018, coupled with emission of ash from the summit craters and (ii) between November 2018 and January 2019, in which the SO_2 signal suddenly increased with average-daily flux values up to ~12,000 tons/day and hourly values up to ~17,000 tons/day, matching the beginning of the effusive activity at the South-East Crater (SEC). This degassing regime continued until 5 January and then gradually returned to the typical degassing values of Etna (being lower than 5000 tons/day). The two degassing phases are separated by a period of moderate and general stability in the emission rate (from April 2018 to October 2019), with values within the range of typical outgassing of Etna and only occasionally exceeding the threshold of warning of 5000 tons/day,

in concomitance with variations in the eruptive activity observed at the summit craters.

The flux of HCl was measured between January 2017 and February 2018 and between mid-December 2018 and January 2019 (fig. S2). Overall, during the first 4 months of 2017, the HCl flux was characterized by a stable regime, with averagely low values (~250 tons/day) featured by episodic increases, some of which (first of March) were particularly intense (1700 tons/day), in conjunction with the onset of effusive/strombolian activity. By the end of June 2017, after the end of the volcanic activity, the HCl flux indicated a generally increasing trend until January 2018, with values up to ~900 tons/day. In the period between December 2018 and January 2019, the geochemical signal showed variations consistent with the eruptive activity. The available data from the second half of December 2018 showed values up to 800 tons/day, followed by a clear decreasing trend that reached values of ~200 tons/day. This decreasing trend was interrupted in the second half of January 2019 with a short-lived higher value matching the stage of variations in the eruptive activity observed at the summit craters.

The CO_2/SO_2 ratio in the volcanic plume is reported in Fig. 2C for the whole investigated period. The ratio showed a general stability at a value of about eight in the first half of 2018 up to the beginning of September. Subsequently, from September 2018 onward, we observed a significant change in the degassing regime, marked by an increase of the CO_2/SO_2 ratio up to values that exceed 30 (Fig. 2C), which can be considered high for the typical CO_2/SO_2 range of variation of the Voragine crater. Although variable, the ratio progressively decreased during November 2018, reaching very low values at the end of the month. After a gap of data due to technical problems, the few available values, recorded some days before the eruption onset, showed medium ratios that increased up to almost 40 in the first days of January 2019. Thereafter, the CO_2/SO_2 ratio, albeit highly variable, began to decrease.

DISCUSSION

In the following, we discuss the inferences of the studied parameters on the magmatic dynamics in the feeding system of Mt. Etna and the relationship with the eruptive activity of December 2018. We start from the signals related to the deeper portions of the magmatic system then moving toward the shallower levels.

The deep recharge

Following Paonita *et al.* (*23*, *37*), the He-Ar-CO_2 systematics of the peripheral gas emissions at Mt. Etna, coupled with chemical and carbon isotope compositions of summit crater fumaroles, provide key insights into magma degassing at depth below the volcano. After the necessary corrections for atmospheric contamination and fractionation processes in surface aquifers, the elemental He/Ar* and Ar*/CO_2 and isotope $^{13}C/^{12}C$ ratios in peripheral and crater gases indicate the occurrence of mixing processes between gases exsolved by deep magmas at pressures greater than 250 to 380 MPa [i.e., from 7 to 12 km below sea level (bsl)] and gases from magma levels at intermediate pressure and depth (130 MPa, i.e., ~3 km bsl) along an open system degassing path (figs. S3 and S4). The corrected He/Ar* and Ar*/CO_2 ratios in the peripheral gases, recorded from 2017 to 2018 (fig. S3), overlap with those reported by Paonita *et al.* (*37*), confirming the above-detailed pressure intervals for the exsolution of these gases. Considering these depths of exsolution and noting that (i) high $^3He/^4He$ ratios are typical of primitive deep magmas (*38*), (ii) the $^3He/^4He$ ratio covaries in very distant sites (several tens of kilometres), supporting a common and deep origin of the variations (*39*, *40*), and (iii) increasing ratios precede the main eruptive phases of Mt. Etna (*23*), it has been concluded that an increase in $^3He/^4He$ isotope ratio indicates an event of magma recharge in a deep (7 to 12 km bsl) and structurally complex portion of the supply system [Fig. 3; (*23*)]. In support of this conclusion, seismic tomographies of Mt. Etna (*41*–*43*) provide evidence of a vertically elongated structure starting from a depth of about 6 km bsl and extending up to 12 km bsl, being a main pathway of magma ascent. Furthermore, the matching of these levels with the depths of both the source of medium-term inflation phases and the crystallization of poorly evolved olivines (Fo78) supports the presence of zones of magma storage (*44*).

In agreement with Paonita *et al.* (*23*), the recharge of primitive magma in a confined reservoir would cause pressurization and an increase in the deep, high $^3He/^4He$ gaseous contribution to the peripheral emissions. This process was physically modeled by Paonita *et al.* (*23*) so that the isotopic signal can be translated into a quantitative

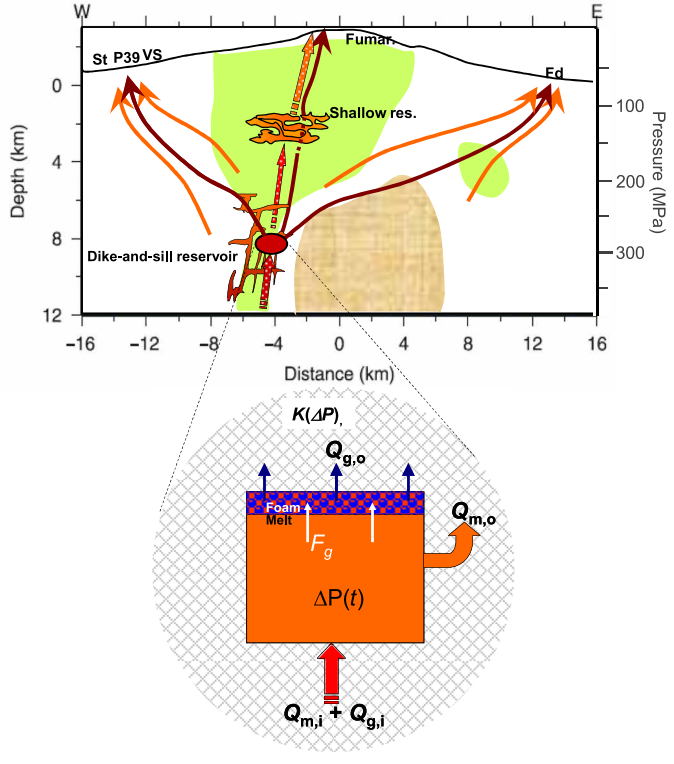

Fig. 3. Sketch of the Etna magmatic system. The shallow (3 km bsl) and deep (7 to 12 km bsl) reservoirs are shown (magma-static rate with 2600 kg/m^2 density has been assumed to relate pressure to depth scale). Dark red and orange dotted arrows indicate magmas with high- and low-$^3He/^4He$ signature, respectively, while the brown and orange arrows indicate likely pathways of the high and low $^3He/^4He$ gaseous components, respectively. The ellipse shows the location of the high $^3He/^4He$ magma body that pressurizes because of deep input. The box diagram provides details on the modeling of this body [hosted in elastic rocks having permeability $K(\Delta P)$], where the overpressure $\Delta P(t)$ is governed by gas and melt input ($Q_{g,i}$ and $Q_{m,i}$), gas and melt output ($Q_{g,o}$ and $Q_{m,o}$), and gas flux from melt to foam (F_g) [modified from (*23*)].

estimation of the pressurization of the deep reservoir zone affected by the recharge of magma and fluids. On the basis of the model, the sampled sites appear to be fed by a mixture of high- and low-$^3He/^4He$ gas endmembers, the former coming from a deep magma reservoir and the latter from intermediate and/or more peripheral reservoirs. When a deep input of magma and fluids pressurizes the deep reservoir, the latter releases large amounts of gases (having the marker of the high $^3He/^4He$ endmember), with flow rate $Q_{g,o}$ (Fig. 3; more details can be found in the Supplementary Materials). The deep gas flow rate is fed by a foam layer that grows at the chamber top, whose volume is controlled by the permeability of the chamber roof, in turn depending on overpressure. The chamber overpressure (ΔP) changes over time as an effect of melt + gas input ($Q_{m,i} + Q_{g,i}$) in the chamber (Fig. 3) and increases toward an asymptotic value (fig. S5). The effect of the gas flow from the melt into the foam (F_g), combined with the resulting overpressure on the magmatic chamber and its effects in increasing wall-rock permeability, produces a sigmoid growth curve of $Q_{g,o}$ (fig. S5). The consequent increases of the $^3He/^4He$ ratio, predicted at a sampled emission site, will display a similar sigmoidal pattern, with the steepest segment of the sigmoid having a slope roughly proportional to the input rate $Q_{m,i}$ (fig.S5). As soon as the deep input ends, the chamber elastically returns to its original volume, while the overpressure decays exponentially similarly to the gas flow rate $Q_{g,o}$ and the $^3He/^4He$ ratio at the site (fig. S5). According to the model, both the rate and time-integrated amount of the recharge can be likewise computed by best fit of the measured $^3He/^4He$ signals (further details in the Supplementary Materials). Roughly speaking, the steeper the observed increase of $^3He/^4He$ ratio over time, the higher the pressurization rate of the chamber and the input rate $Q_{m,i}$ of the magma recharge.

In this conceptual framework, the protracted increase of the He isotope ratio in Fig. 2A suggests that the deep magmatic system of Mt. Etna would have undergone a long recharging process starting in 2017, with the rates as shown in Fig. 4. The period before the summer 2018 would have been characterized by the highest recharge rates [up to 1.7 m^3/s of melt + gas, computed according to the model proposed in (*23*)], and these would still have remained high until the onset of the December 2018 eruption. By contrast, the significant drop in the $^3He/^4He$ ratios during the eruption points to a marked reduction in the deep recharge rate. It is noteworthy that the long recharge period matches an inflationary trend that started in April 2017, more or less when the He isotope ratio began to increase (*31*, *45*, *46*). The main inflation trend was modeled assuming a pressure source located at 6 to 8 km bsl and interpreted as due to the replenishment of a deep reservoir by new arrival of magma, which would have been active for at least 1 year (*31*, *45*). This is entirely consistent with the interpretation based on the He isotope signal, concerning both the depth of the overpressurized reservoir (estimated at 7 to 12 km bsl, according to the measured He/Ar* and Ar^*/CO_2 ratios) and the tracking of the recharge of fresh magma from depth.

By integrating the rate and timing of the deep recharge, the volumes of magma (melt + gas) injected into the deep system have also been estimated. From April 2017 until the beginning of the December 2018 eruption, about 83 Mm^3 would have been injected into the deep system, corresponding to 55 ± 11 Mm^3 of melt, based on the gas/melt ratio of the recharge [about 30%; (*23*)]. It is worth noting that the hypothesized gas proportion greatly exceeds the amount theoretically dissolved in the melt at the pressure of the deep reservoir (*23*). This excess gas would reach the deep reservoir from even deeper levels of the magmatic system. This is in agreement with the hypothesis that Mt. Etna's feeding system would be percolated by a fluid phase decoupled with respect to the melt, probably ascending from the mantle (*47*).

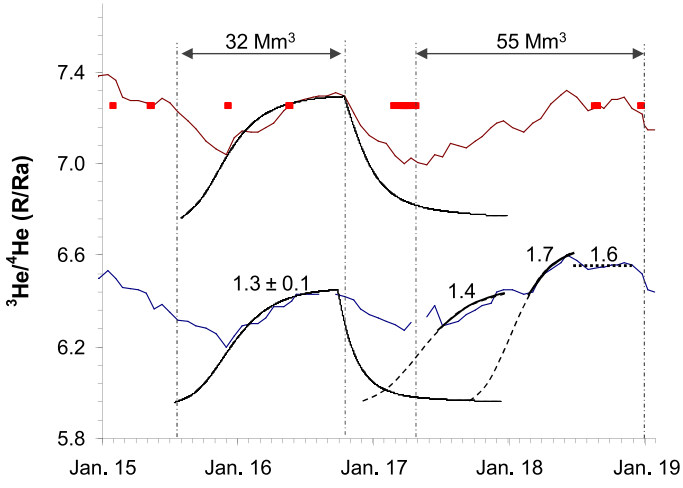

Fig. 4. Modeled magma recharge events based on $^3He/^4He$ isotope ratios. The He isotope signals are from Stadio and P39. Model predictions (sawtooth curves for 2015 to 2016 and sigmoid curves for 2017 to 2018) derived from best fit of the pressurization model to the observed signals; labels next to the model curves are the estimated rates of deep recharge (as m^3/s; estimated uncertainties close to 0.1 m^3/s). Note that higher magma recharge rates give higher increase rates of $^3He/^4He$ ratio, and higher plateau values reached by $^3He/^4He$ too. The flat segment in the second half of 2018 is the plateau value predicted by the model by using a recharge rate of 1.6 m^3/s (see label beside). Double arrows and labels at the top of the plot refer to the integration periods and estimated melt volumes entered into the system. Red bars indicate the eruptive periods.

The above-given volume, if compared to the volume of <3 Mm^3 erupted in the same period (*29*), suggests the accumulation of a large amount of magma in the plumbing system. The calculated amount of accumulated magma is also similar to that estimated by Calvari *et al.* (*33*) on the basis of the constant deep input rate of magma in the Etnean system. These authors suggest that 50 Mm^3 of magma would still have been present in the system after the December eruption, available to be erupted. By looking at the deformation of the volcano, differential interferometric synthetic aperture radar (DInSAR) data indicate a volume of about 30 Mm^3 intruded as a deep dyke between 6 km bsl and the sea level, despite a small amount having been erupted (*27*). Similar estimations (31 ± 7 Mm^3) derive from the high-rate Global Positioning System (GPS) network (*46*). Such a condition of magma accumulation is far from common. For example, in the case of the summer 2015 to October 2016 recharging event (see Fig. 4), our calculations indicate that 32 ± 11 Mm^3 entered the deep system versus ~25 Mm^3 erupted in the same period (*33*), in favor of a much minor (if existing) accumulation of magma.

Magma dynamics at intermediate to shallow levels

With the aim of interpreting the diffuse CO_2 flux from the volcano flanks, as well as the output and composition of the volcanic plume, quantitative modeling of decompressive magmatic degassing of the investigated species is required. These models can predict the pressures at which the species of interest, mainly CO_2 and SO_2 in this study, are exsolved from a decompressing magma. Calculations

have been made for the conditions of melt composition and temperature and gas content of Mt. Etna basaltic magma by Caracausi *et al.* (*40*) and Paonita *et al.* (*37*) for H_2O-CO_2 trace gases system and Aiuppa *et al.* (*48*) for the H_2O-CO_2-SO_2 system.

As concerns CO_2, the models predict its degassing to be limited to pressures greater than 60 to 70 MPa (Fig. 5), namely, at depths higher than 0 km bsl. In this case, the key factor to constrain the magmatic source levels of soil CO_2 emission consists in the areal distribution of the EtnaGAS network measuring this parameter. The location of the network stations extends from peripheral areas, at similar distances and altitudes as the gas vents where we measure the He isotope ratios, to sites much closer to the volcano central axis and having elevations up to 1700 m above sea level (asl). Thus, if the peripheral emissions mainly receive gases from the deep reservoir (with small contributions coming from depths up to 3 km bsl, see above), the EtnaGAS network "sees" an integrated range of depth averagely shallower, whose top is confined by the depth of CO_2 exhaustion in the melt [0 km bsl; see figure 7 in (*25*)]. As already mentioned (see the previous section), open system degassing conditions must occur during magma ascent at these depths, probably thanks to sill-and-dike structures promoting gas-melt decoupling. We note that seismic tomography, GPS modeling, and microgravity studies (*42*, *49*–*51*), together with considerations based on magma buoyancy in the local crust (*52*), suggest the presence of a magma storage volume at 2 to 4 km bsl. More recently, the deformation sources modeled according to the deflation phases of Mt. Etna and the crystallization depth of evolved olivines (Fo75 to Fo76) are compatible with intermediate levels of magma storage at 5 to 6 km bsl (*44*, *53*, *54*). With this in mind, we can conclude that the increase of soil CO_2 flux is linked to the migration of magma and the consequent open system degassing from the deep reservoir, passing through the above-defined storage zone at intermediate depths (3 to 6 km bsl), and lastly reaching the base of the volcanic cone [about 3 km below the craters; (*25*)]. Further transfer of this magma toward more superficial portions of the volcanic edifice is no longer detectable by the EtnaGAS network and is recorded by gradually decreasing CO_2 flux on the volcano flanks (*25*). With this in mind, we can furthermore detail the magma dynamics in the plumbing system by comparing the variations of $^3He/^4He$ ratio versus those of soil CO_2 flux, as the two signals are related to two different windows of depth. Two example cases can make this idea clear. In one case, a recharge of the deep reservoir will cause an increase of $^3He/^4He$ ratio, but if no magma transfer toward the intermediate shallow systems occurs, no increase of soil CO_2 fluxes will be observed. As a second case, we can imagine a massive transfer of magma toward the intermediate shallow systems occurring at a constant recharge rate of the pressurized deep reservoir. We thus would observe (i) a decrease of He isotope ratio due to the decompression of the deep reservoir consequent to the massive magma output from it (even if the deep reservoir continues to receive an input from below) and (ii) an increase (e.g., one or more peaks) of the soil CO_2 flux due to magma transfer throughout the intermediate magmatic system.

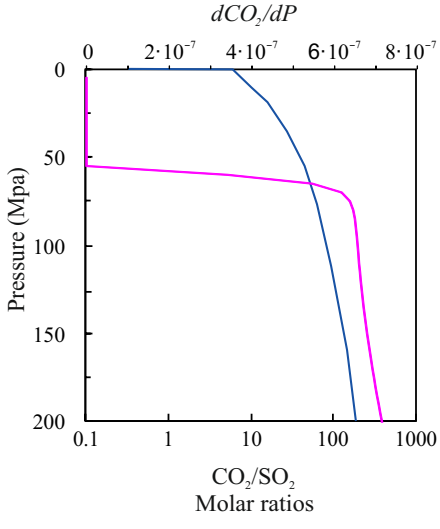

Fig. 5. Degassing paths of Mt. Etna basalt. The blue curve is the modeled CO_2/SO_2 of a gas phase exsolved by closed-system decompression degassing of Mt. Etna basalt, followed by open system degassing at 0.1 MPa (according to 48). Calculations performed at similar conditions by D-Compress code (*69*) do not significantly change the shown trend. In magenta, the dCO_2/dP of melt [as (grams of exsolved CO_2 per gram of melt)/(0.1 × MPa)] throughout open system degassing of Mt. Etna basalt [according to (*37*)].

On this basis, we note that the major peak of CO_2 flux in June 2018 (the first one in the year) paralleled the onset of the decrease of the He isotope ratio from June to August. The magma transfer episode, marked by this peak, would be consequent to the peak of the input and pressurization in the deep system, recorded by the He isotope ratio (see The deep recharge section): The deep reservoir would have reduced its internal overpressure by promoting melt migration toward shallower levels. Accordingly, the subsequent three peaks of CO_2 flux from August to October 2018 match a much slower increase of the He isotope ratio than that characterizing the first half of 2018. It suggests that the intermediate magmatic system was able to efficiently drain magmas from the deep reservoir, somewhat balancing the magma amount entering the deep reservoir from below.

The remarkable decrease of the CO_2 flux, which marked the end of November 2018 and the whole of December 2018, still matches the slight decrease of $^3He/^4He$ ratios. This would suggest that, with the decrease of the overpressure in the deep system, the migration of magma batches, through the reservoir hypothesized at about 3 km bsl and up to the base of the volcanic cone, was much less efficient, and the amount of degassed CO_2 able to feed the soil emissions on the volcano flanks was much lower. As we go on to see, the preeruptive dynamics of magma at very shallow levels could however have contributed, or even played the main role, in draining the overpressure at depth.

In their degassing model for Etnean basalts, Aiuppa *et al.* (*48*) predicted that, while CO_2 exsolves in subcrustal conditions because of its limited solubility in the melt, SO_2 is much more soluble and exsolves in the gaseous phase at very shallower conditions (just anticipated by H_2O exsolution). In particular, in Etnean magmas, the exsolution of SO_2 begins at depths in the range of 3 to 4 km below the craters but becomes more marked in the shallower portions of the magma conduits (2 to 3 km below the craters or less, namely, above the base of the volcanic cone). We recall that the observed strain changes by deep dilatometers during the frequent lava fountains activity at the new SEC (NSEC), constrained a shallow and small-volume source located at a depth of 0 to 0.5 km asl (*55*), where magma storage and accumulation are indicated by the crystallization of Fo70 to Fo73 evolved olivines (*44*). A further storage zone has been inferred at 1 to 2 km asl by means of source localizations of volcanic tremor, overtopped by very shallow levels where gas

bubbles released from the underlying magma batches produce infrasonic signals (*56*). The arrival of magma in the shallow system and the exsolution of H_2O and SO_2 will therefore cause pressurization and a consequent increase of the output of gases (*4*): the greater the amount of entering magma and exsolved gases with respect to the available storage volumes, the greater the pressurization and the increase in the output. On these grounds, high SO_2 fluxes detected in the bulk plume can be linked to the pressurization of the very shallow portion of the volcanic edifice at a depth 2 to 3 km or less below the craters and consequent increased plume outgassing. Also, the variations in the CO_2/SO_2 ratio in the volcanic plume are a consequence of the big contrast of solubility between the two species in the silicate melts (see above). In simple terms, if a magmatic storage zone feeds the plume degassing, the refilling of this magmatic level by a more primitive and volatile-rich basaltic magma corresponds to an increase in the CO_2/SO_2 ratio in plume emissions followed by a rapid decrease in the ratio during the migration of the same magma body toward the surface, as long as SO_2 is largely released (*34*, *48*). The peak values of the CO_2/SO_2 ratios will depend on the pressure (depth) of the magmatic level according to the model curve represented in Fig. 5. More realistically, the degassing by the volcanic plume occurs at the top of the magmatic column, and it can be related to the ascent of a magma batch (melt plus bubbles) up to near atmospheric pressure, where gas finally separates from melt [see (*48*)]. Therefore, closed system conditions of degassing can occur from 0 km asl and along the conduits up to the atmosphere while being followed by open system conditions at 0.1 MPa (favored by cooling and crystallization too) (Fig. 5). In addition, massive gas exsolution at depth due to important magma ascent episodes (e.g., preeruptive) can promote the formation of bubble-rich magma levels, the subsequent bubble-melt separation, and the feeding of the plume degassing with gases coming from depth (*48*). In this case, rising gases can mix with those exsolved along and at the top of the magma column so as to mimic mixing trends rather than pure degassing curves. Because of the very similar theoretical compositions expected by mixing versus degassing (*48*), these two processes are hardly distinguishable within the uncertainties of the measured concentration ratios.

From this viewpoint, the pulsating SO_2 output in the volcanic plume and the low-to medium CO_2/SO_2 values, recorded in the period between July 2017 and May 2018 (Fig. 2), are consistent with modest transfers and degassing of volatile-rich magma batches toward the shallowest portions of the Mt. Etna feeding system (less than 2 km below the craters). These changes were reflected in the occurrence of a short stage of mild eruptive activity at the SEC in summer 2018. By modeling the equivalent magma-flow rate based on the observed bulk SO_2 flux and considering a mean original sulphur content for Etnean magma of 0.3 weight % (*57*), a mean crystal fraction of 30%, and density of degassed magma of 2750 kg/m^3, we estimated that the intracrater explosive strombolian activity experienced in July 2018 was fed by a magma flow of ~2 m^3/s. Eventually, modest variations in magma flow up to ~3 m^3/s led to the transients in the effusive activity observed at the SEC between the 23rd and the 27th of August 2018. Taking into account that the He isotope signal from July 2017 to May 2018 indicates an important magma recharge acting at depth, while SO_2 output and CO_2/SO_2 suggest that the involvement of the shallow system was minor, we hypothesize that the deep magmatic system was still able to accommodate the largest part of the refilling magmas.

By contrast, the observed increases of the CO_2/SO_2 ratio since September 2018 (Fig. 2C) point to the occurrence of a perturbation of the shallow magmatic system, which probably received a contribution of poorly degassed melt of deep origin and rich in CO_2 or, alternatively, of CO_2-rich gases from the overpressurized deep levels. In the first hypothesis (rising magma), the measured CO_2/SO_2 ratios up to 30 would indicate the plume being fed by main degassing events occurring at a depth of about 2 km below the craters (Fig. 5). The values of the SO_2 plume output, being averagely low (Fig. 2D), suggest that those magma levels were not massively pressurized by this arrival, and they were still able to accommodate these melts. As another possibility, the CO_2/SO_2 ratios could have risen after the increased CO_2 flushing from depth, probably paralleled by the incipient magma ascent from the deep plumbing system, without a substantial magma input into the volcano edifice, which would explain the minor/very slight SO_2 degassing in this phase.

It is also notable that the variations of the CO_2/SO_2 ratio in the plume in the period September to November 2018 correlate well with the variations in CO_2 flux from the volcano flanks recorded by the EtnaGAS network. Figure 6 shows a combination of the signals obtained from the two networks, from which almost synchronous variations are observed in the period preceding the start of the volcanic activities recorded in the last months of 2018 (*34*). The coherence of the two signals is the probable consequence of the transfer of deep and CO_2-enriched magma batches toward intermediate (3 km bsl) to shallow portions of the volcano (3 km below the craters), which mark the magmatic recharge phase of Mt. Etna, already highlighted by the He isotopic ratios. As the modeled variations of the helium isotope composition would imply, after the pressurization of the 7 to 12 km deep reservoir (see The deep recharge section), the ascending magma is thought to be associated with a notable amount of gas (*23*).

From the second half of November 2018, the SO_2 flux begins a significant increasing trend, paralleled by the mentioned drop of soil CO_2 flux and the weak $^3He/^4He$ decrease (Figs. 2 and 4). Unfortunately, we have no CO_2/SO_2 plume data up to 20 December, due to technical problems. The above features are consistent with the progressive pressurization inside the volcanic edifice at 2 km below

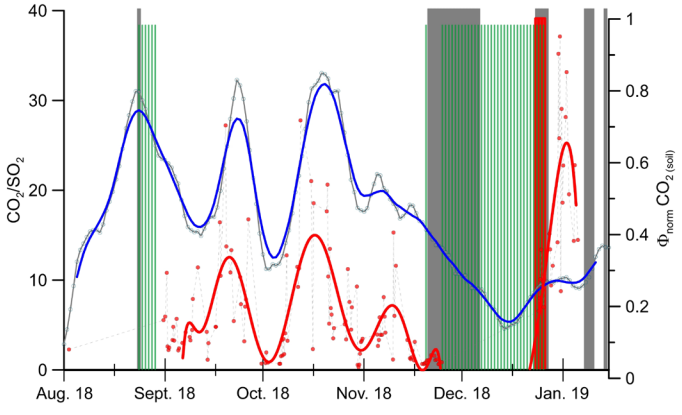

Fig. 6. Plume and soil degassing. Comparison of CO_2/SO_2 ratio of the plume (in red) and the degassing of CO_2 from the soil recorded by the EtnaGAS network (in blue) from September 2018. Red points represent CO_2/SO_2 measurements, while the red curve is a polynomial interpolation of the points. Blue and gray curves are weekly average and daily values of soil CO_2 flux, respectively.

the craters or less. The transfer and accumulation of magma at that level probably contributed to lowering the overpressure at depth, causing the slight decrease of the He isotope ratio, although we cannot exclude that the deep recharge started to decrease according to the time trends of $^3He/^4He$ predicted by the model after (see The deep recharge section) (*23*). The seismic swarm of 6 October could have contributed to catalyzing the ascent of fresh volatile-rich magma reflected in the increase in plume degassing recorded from November 2018, eventually triggering the effusive activity at the SEC on 20 November.

At the onset of the 24 December eruption, the high SO_2 fluxes strongly support the hypothesis that the shallow system at 2 km was heavily pressurized by the new volatile-rich magma. Magma flow up to ~6 m^3/s led to the eruptive event of 24 December 2018 with lava effusion from the eruptive fracture in Valle del Bove. The downward trend in the HCl emission rate from mid-December, together with the high SO_2 values, suggests that this magma did not pond in the summit sector of the volcanic edifice, within 1 km from the craters, but quickly rose to feed the eruption, from a depth compatible with the quantitative degassing of SO_2 (about 2 km from the summit craters). This contributed to preserving its gas content, explaining the particularly forceful nature of this event, and is in agreement with the magma source depth estimated for lava fountains [close to the sea level; (*55*)].

After the eruptive activity of December 2018, the EtnaGAS network recorded low CO_2 degassing at the volcano flanks in January 2019, which is in agreement with the concurrent phase of decrease in the He isotope ratio (Fig. 2). Although the magmatic recharge phase of the deep system seems to have regressed after the eruption onset, unstable degassing conditions still characterized the crater emissions, with highly variable CO_2/SO_2 ratios, accompanied by very high SO_2 fluxes. Given the decaying overpressure in the deep reservoir, the CO_2/SO_2 peaks up to 35 are considered to derive from shallow degassing conditions, in a storage system located 2 km below the craters, still pressurized. Gurrieri *et al.* (*34*) have interpreted the lack of correlation between soil CO_2 degassing and CO_2/SO_2 ratio (see Fig. 6) by an enhanced gas drainage condition from the main volcanic conduits, conjecturing a sort of "chimney effect," which, in turn, is justified by the fact that the volcanic conduits were opened by the ongoing eruption. Moreover, this phase of shallow turmoil can also explain the phenomena of intermittent and frequent emission of ashes from the summit craters in that period (*33*).

Table 1. Average CO_2/SO_2 ratios, SO_2 and CO_2 fluxes, and cumulative CO_2 amounts. The three selected subperiods cover the time span 2017 to 2018. For each subperiod, CO_2/SO_2 ratio and SO_2 flux are the average of all the daily measurements available, while CO_2 flux has been computed by combining daily SO_2 fluxes and CO_2/SO_2 ratios when both the measurements were available and after averaging the values. The cumulative CO_2 has been calculated by integrating the average daily CO_2 flux for the whole subperiod, while the total CO_2 is the sum of the three subperiods. Average uncertainties on cumulative CO_2 have been evaluated to be 32%.

Subperiod	SO_2 flux (ktons/day)	CO_2/SO_2	CO_2 flux (ktons/day)	CO_2 (Mtons)
September–December 2017	3.20	1.66	5.18	0.63 ± 0.18
January–24 December 2018	3.53	4.57	13.44	4.80 ± 1.44
25 December 2018–5 January 2019	8.36	11.86	100.75	1.11 ± 0.33
Total				**6.54 ± 1.96**

Combining the parameters: Gas imbalance in the magmatic system

The SO_2 flux and CO_2/SO_2 ratios can be combined to achieve a rough estimation of the CO_2 flux from the volcanic plume, which quantifies the output of CO_2 from the volcanic system [excepting additional amounts diffused by soil and dissolved in aquifers, which can be estimated within 10% of the plume degassing; (*58*)]. On the other hand, we have the capability to estimate the input of melt + gas by the deep magma recharge into the system. This means that a gas balance can be assessed by combining the quantitative evaluation of input and output coming from the investigated signals. In detail, we focused on the preeruptive period starting from September 2017, where CO_2/SO_2 values are available without important gaps. The period was divided into three subintervals for which an average value of CO_2/SO_2 ratio and SO_2 flux was considered to be representative (Table 1). These periods spanned: (i) September to December 2017; (ii) January to 24 December 2018; and (iii) 25 December to 5 January 2019, whose average CO_2 fluxes were 0.6, 4.8, and 1.1 Mtons, respectively, with 32% estimated maximum uncertainty (achieved by error propagation of coupled SO_2 flux and CO_2/SO_2 uncertainties). On the basis of these data, a cumulative curve of CO_2 output from the system was computed for the whole period from September 2017 to January 2019 (Fig. 7).

For the gas input, starting from the estimated gas/melt ratio of the recharge, we can convert the computed melt recharge rates represented in Fig. 4 into gas recharge rates and consequently can compute a cumulative curve of gas input into the deep system over time. Taking into account the H_2O and CO_2 proportion of this magmatic

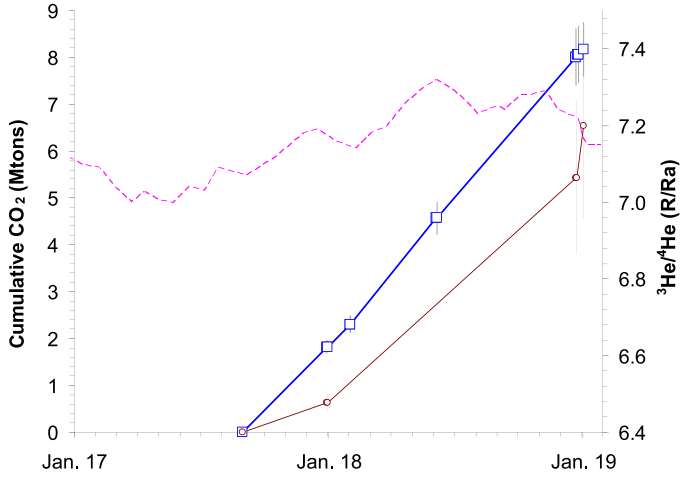

Fig. 7. Cumulative input and output of CO_2. Cumulative amount of CO_2 inputted into the magmatic system from depth (blue line) and outputted from plume degassing (brown line). The uncertainties for input CO_2 were computed by the average error in the deep input rate (0.1 m^3/s; see Fig. 4), while for output CO_2 as in Table 1. He isotope signal from the P39 site is also shown (pink dashed line).

gas (*23*, *37*), we readily obtain a cumulative curve for CO_2. This calculation has been done by starting from September 2017 up to January 2019, the same as the gas output (Fig. 7). Looking at the He isotope signal, the preeruptive recharge event started before September 2017; therefore, the amount of CO_2 that entered the system must be regarded as a minimum.

What clearly emerges from this gas balance is that the cumulative CO_2 amount that entered the system was much higher than the corresponding CO_2 degassed from the plume, and this imbalance reached its peak just before the eruption onset. At that moment, the difference between input (8.0 ± 0.6 Mtons) and output CO_2 (5.4 ± 1.6 Mtons) suggests that about 2.6 Mtons of this gas has been accumulated in the magmatic system and probably fueled the paroxysmal explosive activity of 24 December and the related phenomena, such as intrusions, seismicity, ground deformation, and fracture opening. While this imbalance required almost 15 months to build up, it dropped by almost 1 Mton in the few days following the eruption onset, explaining the impressive syn- and posteruptive degassing of the volcano. When looking at these results, what emerges is the exceptional condition of the volcano at the moment of the 2018 Christmas eruption.

The evolution of the volcano related to the eruption

Our analysis and interpretation of the signals coming from the geochemical monitoring at Mt. Etna allows recognizing three main phases related to the 24 December eruption. These are sketched out in Fig. 8 and explained below.

Recharge phase: The $^3He/^4He$ isotope ratio in the gaseous emissions at the base of the volcano increased from April 2017. After the peak reached in June 2018, they showed stable values on medium-high levels until November. This suggests that the contribution of primitive magma into the deep system (7 to 12 km bsl) was sustained for 5 to 6 months, albeit with rates lower than the presummer ones, resulting in conditions of substantial pressurization at the time of the start of the eruptive activity on 24 December.

The progressive pressurization at depth would be the cause of a sequence of pulsating events of ascent of either magma batches or CO_2-rich fluids from the deep toward the intermediate and shallow

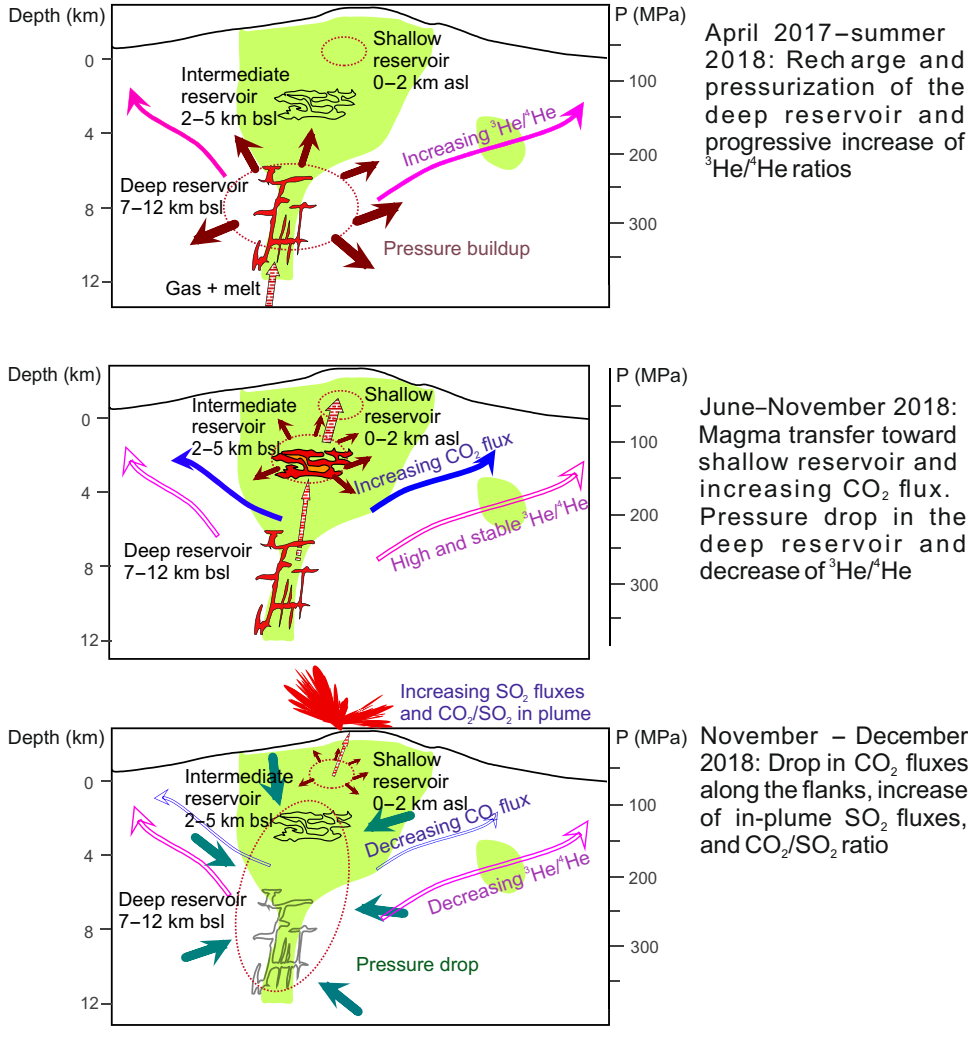

Fig. 8. Sketch of the Mt Etna magmatic system feeding the December 2018 eruption. From the top, the long-lasting magma and fluid recharge at depth, the magma transfer throughout the intermediate system up to the base of the volcanic edifice from June to November 2018, and last, the coupled pressurization of the conduit storage system (2 to 3 km below the craters) and decompression of the deep and intermediate reservoirs.

portions of the magmatic system. These events are clearly recognizable as different phases of marked increase in the diffused CO_2 flux from the soils from June to October 2018, which parallels the pulsating increase in the CO_2/SO_2 ratio in the plume and confirm the increased contribution of deeply released CO_2-rich fluids and/or less degassed magmas. The observed phenomena at the summit craters in the same period (episodes of Strombolian and effusive activity) would be attributable to the same process.

Pre- and syneruptive phase: Starting from November 2018, the marked decrease in CO_2 emissions from the volcano flanks and the slight decrease of the $^3He/^4He$ ratio would indicate that the overpressurization of the deep system was probably decreasing. By contrast, the high pre- and syneruptive SO_2 fluxes, coupled with medium-to-high values of CO_2/SO_2, indicate that the shallow system was progressively accumulating poorly degassed magma and was consequently pressurizing. It is plausible that the two simultaneous processes are due to magma transfer from the base of the volcano edifice to shallower portions. The very shallow dynamics would explain the contemporary vigorous degassing activity.

Posteruptive phase: The significant drop in the $^3He/^4He$ ratio, which began during the eruption and continued in the following days, suggests that the system certainly decompressed as a consequence of the eruption. Although with different timing, this decompressive event involved the whole magmatic system at all levels, as indicated by the persistently low CO_2 fluxes at the volcano flanks, followed by the decreasing CO_2/SO_2 ratios and SO_2 output of the plume starting from January 2019. Besides this eruption-induced decompression, we can also hypothesize that the deep magmatic recharge gradually became exhausted after the eruption, as the general decline of the monitored parameters persisted in the following months. Accordingly, no further eruptive activity followed the explosive event of 24 December.

Last, we attempted a time-dependent balance between the amount of CO_2 that entered the system from depth and that released by plume degassing. This is an exceptional possibility at Mt. Etna, where the deep melt + gas input can be estimated by quantitative modeling based on the He isotope ratio signal, and the plume gas output is continuously measured. The result suggests that, by the onset of the 24 December eruption, the magmatic system had already accumulated an impressive quantity of CO_2, which could not be efficiently released by inter-eruptive volcano degassing, and this reasonably provided the energy required to intrude the two dikes, to open the eruptive fracture, to stretch the volcano thereby reactivating the East flank sliding, and finally to drive the paroxysmal explosion. Beyond its usefulness in the discussion on the exceptional characteristics of the 2018 "Christmas eruption," the procedure used to estimate the gas balance may also be applied more broadly, for example, in the prediction of eruptive potential and therefore hazard evaluation during volcanic crises.

MATERIALS AND METHODS

The eruption of 24 to 27 December 2018 at Mount Etna

In July 2018, a weak explosive activity at Bocca Nuova (BN) and the North-East crater (NEC) marked the resumption of Mt. Etna activity, leading to the eruptive episode of 23 to 28 August 2018 consisting of Strombolian explosions and lava flows at the NSEC. Persistent and mild Strombolian activity and ash emission continued at BN, NEC, and NSEC during autumn 2018, coupled with a constant inflation of the volcano edifice (*59*). On the morning of 24 December 2018, an eruptive fissure opened on the side of NSEC at about 3100 m asl, preceded by a seismic swarm that occurred under the summit area and the upper SE flank (*27*). The fracture spread rapidly to the south-east, reaching an altitude of 2400 m asl with a total length of about 2 km. The explosive activity, sustained by the aforementioned crack, as well as by BN and NEC, fueled an impressive plume of gas and ash and a lava fountain (*33*). A series of vents along the fissure fed a remarkable lava outflow in the Valle del Bove, which, however, ended after a few days. Despite the short duration and extent of lava field, the seismic swarm accompanying the eruptive phase was very powerful, with dozens of events with a moment magnitude (M_w) > 3 localized beneath the upper part of the volcano (*27*, *32*). The seismic swarm lasted for many days, with a continuously decreasing number of daily events and magnitude. Apart from the seismic swarm, an M_w = 4.9 earthquake struck the lower SE flank of Mt. Etna on 26 December at 02:19 GMT (*32*). The ground deformation pattern was also wide and intense. The modeling of satellite DInSAR deformation data suggested an upward movement of ~30 Mm^3 magma batch intruded along a North-South feeder dike starting from ~4 km bsl (*27*). The dyke aborted its ascent at about the sea level but stretched the edifice and triggered the opening of the eruptive fracture fed by a shallower and smaller dyke (*27*, *28*). A second dyke was modeled using data from multidisciplinary continuous deformation networks [continuous GPS, borehole strainmeters, and tiltmeters; (*31*)] and high-rate GPS data (*59*), which intruded southward with respect to the previous dyke during a later syneruptive phase but did not reach the surface. The effusion ended on the evening of 26 December, after just 2 days, during which 1.4 ± 0.5 Mm^3 of material as summit outflows and 0.85 ± 0.3 Mm^3 as lateral flows were emitted (*29*). As a consequence of the tensile action of the intrusion, the ground deformation pattern showed clear evidence of the reactivation of the well-known eastward sliding of the eastern flank of Mt. Etna (*31*). This is also testified by the seismicity released in response to the flank movement during the days following the eruption (*32*).

Investigated dataset

The investigated data in this work come from continuous monitoring networks installed on Mt. Etna and from discrete samplings carried out at specific sites (Fig. 1), as detailed in the following. The monitoring facilities are supported by the Istituto Nazionale di Geofisica e Vulcanologia (INGV) - Italian Civil Protection Department (DPC) joint surveillance program.

Chemical and isotope composition of peripheral gases

Gases discharged from five emissions around the periphery of Mt. Etna volcano have been geochemically monitored since 1996 (*39*, *40*). Gas samples are taken from the Vallone Salato and Stadio di Paternò mud volcanoes (hereafter called VS and St, respectively) and a soil gas emission near the village of Paternò (P39) on the southern flank of the volcano, the bubbling water channel of Fondachello (Fd) along the East coast, and the CO_2 exploitation wells of Naftia (hereafter called Nf), located on the Hyblean foreland 40 km away from the volcano, along a northeast-southwest trending fault. The discharged gases are collected by means of a stainless-steel funnel in the case of mud volcanoes and bubbling gases or by a probe inserted 50 cm into the emission orifice for soil gases or directly connected to the well head at Naftia. Two-way Pyrex bottles with vacuum valves at both ends are connected to the system and

used as sample containers. All five sites have usually been sampled at a rate of once every 2 weeks, which increased to one or even two samples per week during periods of unrest of the volcano (*39*, *40*, *60*, *61*). Chemical concentrations of He, N_2, O_2, H_2, CO, CH_4, CO_2, and isotope compositions of He and Ar are measured by standard analytical techniques (*23*, *37*, *39*, *40*, *60*, *61*). Gas chemical composition was determined by means of a PerkinElmer 8500 gas chromatograph equipped with a 4-m Carbosieve 5A column and double detector (flame ionization detector and hot wire detector). Abundances and isotope compositions of Ar were determined with a multicollector mass spectrometer (Argus). Abundances and isotope compositions of He and $^4He/^{20}Ne$ ratio were analyzed by means of a split flight tube mass spectrometer (Helix SFT) where He and Ne were separately admitted after cryogenic separation. All the analyses were carried out within 1 week from the sampling to prevent any problems of gas leakage and fractionation that can modify the chemistry of the sampled gases before their analysis. The measured $^3He/^4He$ isotope ratio is expressed as R/Ra notation, Ra being the He isotope ratio in the atmosphere.

At the peripheral sites, the main gas species in these emissions is CO_2 except for Fd, where it is CH_4, with minor and trace amounts of other species. Shallow interaction of gas with aquifers modifies their geochemistry, so that the original magmatic signature needs to be restored by using models of gas-aquifer interaction (*37*, *40*). This secondary process has no detectable effects on He isotope ratios of the vents (*40*). Air addition must also be quantified and removed, especially when the magmatic Ar content is retrieved. $^{40}Ar/^{36}Ar$ isotope ratio can suitably be used to estimate this air-corrected Ar abundance, hereafter expressed as Ar* (*37*).

Continuous measurements of soil CO_2 flux from the volcano flanks

The diffuse degassing of CO_2 from the flanks of the volcano is measured by the INGV EtnaGAS network, which consists of 14 automatic stations (Fig. 1). CO_2 flux is measured according to the dynamic method [(*62*, *24*) and reference therein]. The network provides an almost homogeneous coverage of the volcano flanks and has been located specifically at sites characterized by significant soil CO_2 emissions. Each monitoring station, entirely developed at INGV-Palermo (INGV-PA), is able to acquire CO_2 soil flux, atmospheric temperature, pressure, humidity, rain, and wind speed and direction. The data are recorded hourly, stored locally, and transmitted daily to the INGV-PA by Global System for Mobile Communications (GSM) or radio links. Soil CO_2 degassing signals can be influenced by meteorological variations (*25*); thus, it is necessary to filter signals from these influences. To this end, a filtering protocol, "MAFILT" (Moving Average FILTer), is automatically applied to the data recorded by the EtnaGAS network to remove interference due to meteorological variations (*34*). We consider here the data processing approach proposed in Liuzzo *et al.* (*25*) to obtain a unique CO_2 flux signal from all the monitoring stations of the network. In this method, each time series from all the stations is filtered for the meteorological parameters and/or seasonal variations. To compare the amplitude of the CO_2 flux variation from different stations, each soil CO_2 flux series is normalized within the range of 0 to 1, and last, all the time series from each station are added together, and the final sum is normalized again within the interval 0 to 1. The data were normalized by referring to the period January 2011 to January 2019. The results are shown as Φ_{Norm}, representing the total soil CO_2 flux amplitude variations over time.

SO_2 and HCl fluxes from the volcanic plume

Continuous remote measurements of bulk SO_2 flux in the volcanic plume are carried out by the Osservatorio Etneo (INGV-OE) through the differential optical absorption spectroscopy (DOAS) scanning spectrometer INGV network FLAME and the discrete measurements of the SO_2/HCl molar ratios performed by solar occultation FTIR technique [Fourier transform infrared spectroscopy; (*63*)]. The latter also provides the HCl flux value by combining the SO_2/HCl ratios determined by FTIR with the flux of SO_2 detected by the FLAME network. The FLAME consists of nine autonomous ultraviolet (UV) scanning spectrometer stations installed at a mean altitude of ~900 m asl on the flanks of Mt. Etna and at a mean distance of ~14 km from the summit craters (*19*, *64*, *65*). Recorded UV open-path spectra are inverted applying the DOAS technique using a modeled clear-sky spectrum rather than a measured spectrum as in the classic DOAS technique (*64*). SO_2-scanned volcanic-plume profiles are then transmitted in real time to the INGV-OE in Catania, where they undergo data-quality evaluation before being reduced in SO_2 mass emission. Average uncertainty in SO_2 flux in our dataset is around ±25%.

CO_2/SO_2 ratio in the volcanic plume

The measurements of the CO_2/SO_2 ratio of the plume at Etna are acquired by a fully automated permanent MultiGAS station (entirely designed by INGV-PA) located on the northern edge of the Voragine crater. The acquired data, temporarily stored in an internal memory board, are telemetered daily via radio-modem bridge back to Palermo, where they are automatically postprocessed (using an INGV custom-made software) to calculate the in-plume CO_2/SO_2 ratios and lastly validated using the dedicated software Ratiocalc (*66*). The MultiGas instrument is equipped with an nondispersive infrared (NDIR) spectrophotometer for detecting CO_2 concentrations (Gascard Edinburgh Sensors) in the range of 0 to 3000 ppm/v and an electrochemical sensor for SO_2 (City Technology Ltd.) with a range of 0 to 200 ppm/v. The station acquires gas concentrations over a period of 30 min (at 1 Hz), four times per day [see (*48*, *67*, *68*) for details]. Average uncertainty in CO_2/SO_2 flux in our dataset is around ±20%.

SUPPLEMENTARY MATERIALS

Supplementary material for this article is available at https://science.org/doi/10.1126/sciadv.abg6297

REFERENCES AND NOTES

1. H. E. Huppert, A. W. Woods, The role of volatiles in magma chamber dynamics. *Nature* **420**, 493–495 (2002).
2. L. Caricchi, C. Annen, J. Blundy, G. Simpson, V. Pinel, Frequency and magnitude of volcanic eruptions controlled by magma injection and buoyancy. *Nat. Geosci.* **7**, 126–130 (2014).
3. S. Tait, C. Jaupart, S. Vergniolle, Pressure, gas content and eruption periodicity of a shallow crystallising magma chamber. *Earth Planet. Sci. Lett.* **92**, 107–123 (1989).
4. A. W. Woods, H. E. Huppert, On magma chamber evolution during slow effusive eruptions. *J. Geophys. Res.* **108**, 2403 (2003).
5. C. Oppenheimer, T. P. Fischer, B. Scaillet, Volcanic degassing: Process and impact, in *Treatise on Geochemistry (Second Edition)* (Elsevier, 2014), pp. 111–179.
6. J. F. Luhr, I. S. E. Carmichael, J. C. Varekamp, The 1982 eruptions of El Chichón Volcano, Chiapas, Mexico: Mineralogy and petrology of the anhydritebearing pumices. *J. Volcanol. Geotherm. Res.* **23**, 69–108 (1984).
7. P. Francis, C. Oppenheimer, D. Stevenson, Endogenous growth of persistently active volcanoes. *Nature* **366**, 554–557 (1993).
8. K. Kazahaya, H. Shinohara, G. Saito, Excessive degassing of Izu-Oshima volcano: Magma convection in a conduit. *Bull. Volcanol.* **56**, 207–216 (1994).
9. T. M. Gerlach, K. A. McGee, Total sulfur dioxide emissions and pre-eruption vapor-saturated magma at Mount St. Helens, 1980–88. *Geophys. Res. Lett.* **21**, 2833–2836 (1994).

10. P. Allard, B. Behncke, S. D'Amico, M. Neri, S. Gambino, Mount Etna 1993–2005: Anatomy of an evolving eruptive cycle. *Earth Sci. Rev.* **78**, 85–114 (2006).
11. P. J. Wallace, From mantle to atmosphere: Magma degassing, explosive eruptions, and volcanic volatile budgets, in *Melt Inclusions in Volcanic Systems: Methods, Applications and Problems*, B. De Vivo, R. J. Bodnar, Eds. (Elsevier Science, Developments in Volcanology, 2003), vol. 5, pp. 105–127.
12. H. Shinohara, Excess degassing from volcanoes and its role on eruptive and intrusive activity. *Rev. Geophys.* **46**, RG4005 (2008).
13. T. Christopher, M. Edmonds, M. C. S. Humphreys, R. A. Herd, Volcanic gas emissions from Soufrière Hills Volcano, Montserrat 1995–2009, with implications for mafic magma supply and degassing. *Geophys. Res. Lett.* **37**, L00E04 (2010).
14. R. Moretti, N. Métrich, I. Arienzo, V. Di Renzo, A. Aiuppa, P. Allard, Degassing vs. eruptive styles at Mt. Etna volcano (Sicily, Italy). Part I: Volatile stocking, gas fluxing, and the shift from low-energy to highly explosive basaltic eruptions. *Chem. Geol.* **482**, 1–17 (2018).
15. A. J. Moffat, M. M. Millán, The applications of optical correlation techniques to the remote sensing of SO_2 plumes using sky light. *Atmos. Environ.* **5**, 677–690 (1971).
16. P. Mouginis-Mark, J. Crisp, J. Fink, *Remote Sensing of Active Volcanism, Volume 166* (American Geophysical Union, Washington DC, 2000), Geophysical Monograph Series.
17. G. Williams-Jones, J. Stix, C. Hickson, The COSPEC Cookbook: Making SO_2 measurements at active volcanoes, in *Methods in Volcanology* (IAVCEI, 2008), vol. 1.
18. A. La Spina, M. Burton, G. G. Salerno, Unravelling the processes controlling gas emissions from the central and northeast craters of Mt. Etna. *J. Volcanol. Geotherm. Res.* **198**, 368–376 (2010).
19. S. Calvari, G. G. Salerno, L. Spampinato, M. Gouhier, A. La Spina, E. Pecora, A. Harris, P. Labazuy, E. Biale, E. Boschi, An unloading foam model to constrain Etna's 11-13 January 2011 lava fountaining episode. *J. Geophys. Res. Solid Earth* **116**, B11207 (2011).
20. N. Huret, C. Segonne, S. Payan, G. G. Salerno, V. Catoire, Y. Ferrec, T. Roberts, A. P. Fossi, D. Rodriguez, L. Croizé, S. Chevrier, S. Langlois, A. La Spina, T. Caltabiano, Infrared hyperspectral and ultraviolet remote measurements of volcanic gas plume at Mt Etna during IMAGETNA Campaign. *Remote Sens.* **11**, 1175 (2019).
21. F. Cannavò, A. G. Camacho, P. J. González, M. Mattia, G. Puglisi, J. Fernández, Real time tracking of magmatic intrusions by means of ground deformation modeling during volcanic crises. *Sci. Rep.* **5**, 10970 (2015).
22. P. M. Gregg, S. L. De Silva, E. B. Grosfils, Thermomechanics of shallow magma chamber pressurization: Implications for the assessment of ground deformation data at active volcanoes. *Earth Planet. Sci. Lett.* **384**, 100–108 (2013).
23. A. Paonita, A. Caracausi, M. Martelli, A. Rizzo, Temporal variations of helium isotopes in volcanic gases quantify pre-eruptive refill and pressurization in magma reservoirs: The Mount Etna case. *Geology* **44**, 499–502 (2016).
24. S. Gurrieri, M. Liuzzo, G. Giudice, Continuous monitoring of soil CO_2 flux on Mt. Etna: The 2004–2005 eruption and the role of regional tectonics and volcano tectonics. *J. Geophys. Res.* **113**, B09206 (2008).
25. M. Liuzzo, S. Gurrieri, G. Giudice, G. Giuffrida, Ten years of soil CO_2 continuous monitoring on Mt. Etna: Exploring the relationship between processes of soil degassing and volcanic activity. *Geochem. Geophys. Geosyst.* **14**, 2886–2899 (2013).
26. G. G. Salerno, M. Burton, G. Di Grazia, T. Caltabiano, C. Oppenheimer, Coupling between magmatic degassing and volcanic tremor in basaltic volcanism. *Front. Earth Sci.* **6**, 157 (2018).
27. A. Bonforte, F. Guglielmino, G. Puglisi, Large dyke intrusion and small eruption: The December 24, 2018 Mt. Etna eruption imaged by Sentinel-1 data. *Terra Nova* **31**, 405–412 (2019).
28. V. De Novellis, S. Atzori, C. De Luca, M. Manzo, E. Valerio, M. Bonano, C. Cardaci, R. Castaldo, D. Di Bucci, M. Manunta, G. Onorato, S. Pepe, G. Solaro, P. Tizzani, I. Zinno, M. Neri, R. Lanari, F. Casu, DInSAR analysis and analytical modelling of Mount Etna displacements: The December 2018 volcano-tectonic crisis. *Geophys. Res. Lett.* **46**, 5817–5827 (2019).
29. M. Laiolo, M. Ripepe, C. Cigolini, D. Coppola, M. Della Schiava, R. Genco, L. Innocenti, G. Lacanna, E. Marchetti, F. Massimetti, M. C. Silengo, Space- and ground-based geophysical data tracking of magma migration in shallow feeding system of Mount Etna volcano. *Remote Sens.* **11**, 1182 (2019).
30. E. Giampiccolo, O. Cocina, P. De Gori, C. Chiarabba, Dyke intrusion and stress-induced collapse of volcano flanks: The example of the 2018 event at Mt. Etna (Sicily, Italy). *Sci. Rep.* **10**, 6373 (2020).
31. M. Aloisi, A. Bonaccorso, F. Cannavò, G. Currenti, S. Gambino, The 24 december 2018 eruptive intrusion at Etna volcano as revealed by multidisciplinary continuous deformation networks (CGPS, Borehole Strainmeters and Tiltmeters). *J. Geophys. Res. Solid Earth* **125**, e2019JB019117 (2020).
32. S. Alparone, G. Barberi, E. Giampiccolo, V. Maiolino, A. Mostaccio, C. Musumeci, A. Scaltrito, L. Scarfì, T. Tuvè, A. Ursino, Seismological constraints on the 2018 Mt. Etna (Italy) flank eruption and implications for the flank dynamics of the volcano. *Terra Nova* **32**, 334–344 (2020).
33. S. Calvari, G. Bilotta, A. Bonaccorso, T. Caltabiano, A. Cappello, C. Corradino, C. Del Negro, G. Ganci, M. Neri, E. Pecora, G. G. Salerno, L. Spampinato, The VEI 2 Christmas 2018 Etna eruption: A small but intense eruptive event or the starting phase of a larger one? *Remote Sens.* **12**, 905 (2020).
34. S. Gurrieri, M. Liuzzo, G. Giuffrida, G. Boudoire, The first observations of CO_2 and CO_2/SO_2 degassing variations recorded at Mt. Etna during the 2018 eruptions followed by three strong earthquakes. *Ital. J. Geosci.* **140**, 95–106 (2021).
35. T. Caltabiano, M. Burton, S. Giammanco, P. Allard, N. Bruno, F. Murè, R. Romano, *Volcanic Gas Emissions from the Summit Craters and Flanks of Mt. Etna, 1987–2000* (American Geophysical Union, 2004), *Geophysical Monograph Series*, pp. 111–128.
36. L. Spampinato, M. Sciotto, A. Cannata, F. Cannavo, A. La Spina, M. Palano, G. G. Salerno, E. Privitera, T. Caltabiano, Multiparametric study of the February–April 2013 paroxysmal phase of Mt. Etna New South-East crater. *Geochem. Geophys. Geosyst.* **16**, 1932–1949 (2015).
37. A. Paonita, A. Caracausi, G. Iacono-Marziano, M. Martelli, A. Rizzo, Geochemical evidence for mixing between fluids exsolved at different depths in the magmatic system of Mt Etna (Italy). *Geochim. Cosmochim. Acta* **84**, 380–394 (2012).
38. C. J. Ballentine, P. G. Burnard, Production, release and transport of noble gases in the continental crust. *Rev. Mineral. Geochem.* **47**, 481–538 (2002).
39. A. Caracausi, R. Favara, S. Giammanco, P. M. Nuccio, A. Paonita, G. Pecoraino, A. Rizzo, Mount Etna: Geochemical signals of magma ascent and unusually extensive plumbing system. *Geophys. Res. Lett.* **30**, 1057–1060 (2003).
40. A. Caracausi, F. Italiano, P. M. Nuccio, A. Paonita, A. Rizzo, Evidence of deep magma degassing and ascent by geochemistry of peripheral gas emissions at Mt. Etna (Italy): Assessment of the magmatic reservoir pressure. *J. Geophys. Res.* **108**, 2463–2484 (2003).
41. C. Chiarabba, A. Amato, E. Boschi, F. Barberi, Recent seismicity and tomographic modeling of the Mount Etna plumbing system. *J. Geophys. Res.* **105**, 10923–10938 (2000).
42. P. De Gori, C. Chiarabba, D. Patané, *Qp* structure of Mount Etna: Constraints for the physics of the plumbing system. *J. Geophys. Res.* **110**, B05303 (2005).
43. D. Patanè, G. Barberi, O. Cocina, P. De Gori, C. Chiarabba, Time-resolved seismic tomography detects magma intrusions at Mount Etna. *Science* **313**, 821–823 (2006).
44. A. Cannata, G. Di Grazia, M. Giuffrida, S. Gresta, M. Palano, M. Sciotto, F. Zuccarello, Space-time evolution of magma storage and transfer at Mt.Etna volcano (Italy): The 2015–2016 reawakening of Voragine crater. *Geochem. Geophys. Geosyst.* **19**, 471–495 (2018).
45. A. M. Borzi, M. Giuffrida, F. Zuccarello, M. Palano, M. Viccaro, The Christmas 2018 Eruption at Mount Etna: Enlightening how the volcano factory works through a multiparametric inspection. *Geochem. Geophys. Geosyst.* **21**, e2020GC009226 (2020).
46. M. Mattia, V. Bruno, E. Montgomery-Brown, D. Patanè, G. Barberi, M. Coltelli, Combined Seismic and Geodetic Analysis Before, during, and after the 2018 Mount Etna Eruption. *Geochem. Geophys. Geosyst.* **21**, e2020GC009218 (2020).
47. C. Ferlito, Mount Etna volcano (Italy). Just a giant hot spring! *Earth Sci. Rev.* **177**, 14–23 (2018).
48. A. Aiuppa, R. Moretti, C. Federico, G. Giudice, S. Gurrieri, M. Liuzzo, P. Papale, H. Shinohara, M. Valenza, Forecasting Etna eruptions by real-time observation of volcanic gas composition. *Geology* **35**, 1115–1118 (2007).
49. M. Aloisi, O. Cocina, G. Neri, B. Orecchio, E. Privitera, Seismic tomography of the crust underneath the Etna volcano, Sicily. *Phys. Earth Planet. Inter.* **134**, 139–155 (2002).
50. A. Bonaccorso, P. M. Davis, *Modeling of Ground Deformation Associated with Recent Lateral Eruptions: Mechanics of Magma Ascent and Intermediate Storage at Mt Etna* (American Geophysical Union, Washington DC, 2004), Geophysical Monograph Series, vol. 143, pp. 293.
51. G. Budetta, D. Carbone, F. Greco, H. Rymer, *Microgravity Studies at Mount Etna (Italy)* (American Geophysical Union, Washington DC, 2004), Geophysical Monograph Series. vol. 143, pp. 221.
52. R. A. Corsaro, M. Pompilio, Buoyancy-controlled eruption of magmas at Mt Etna. *Terra Nova.* **16**, 16–22 (2004).
53. A. Bonforte, A. Bonaccorso, F. Guglielmino, M. Palano, G. Puglisi, Feeding system and magma storage beneath Mt. Etna as revealed by recent inflation/deflation cycles. *J. Geophys. Res.* **113**, B05406 (2008).
54. M. Aloisi, A. Bonaccorso, F. Cannavò, G. M. Currenti, Coupled short- and medium-term geophysical signals at Etna volcano: Using deformation and strain to infer magmatic processes from 2009 to 2017. *Front Earth Sci.* **6**, 109 (2018).
55. A. Bonaccorso, S. Calvari, G. Currenti, C. Del Negro, G. Ganci, A. Linde, R. Napoli, S. Sacks, A. Sicali, From source to surface: Dynamics of Etna's lava fountains investigated by continuous strain, magnetic, ground and satellite thermal data. *Bull. Volcanol.* **75**, 690 (2013).
56. D. Patanè, A. Aiuppa, M. Aloisi, B. Behncke, A. Cannata, M. Coltelli, G. Di Grazia, S. Gambino, S. Gurrieri, M. Mattia, G. Salerno, Insights into magma and fluid transfer at Mount Etna by a multiparametric approach: A model of the events leading to the 2011 eruptive cycle. *J. Geophys. Res. Solid Earth* **118**, 3519–3539 (2013).
57. N. Spilliaert, P. Allard, N. Métrich, A. V. Sobolev, Melt inclusion record of the conditions of ascent, degassing, and extrusion of volatile-rich alkali basalt during the powerful 2002 flank eruption of Mount Etna (Italy). *J. Geophys. Res.* **111**, B04203 (2006).

58. W. D'Alessandro, S. Giammanco, F. Parello, M. Valenza, CO_2 output and $\delta^{13}C(CO_2)$ from Mount Etna as indicators of degassing of shallow asthenosphere. *Bull. Volcanol.* **58**, 455–458 (1997).
59. F. Cannavo', M. Sciotto, A. Cannata, G. Di Grazia, An integrated geophysical approach to track magma intrusion: The 2018 Christmas eve eruption at Mount Etna. *Geophys. Res. Lett.* **46**, 8009–8017 (2019).
60. A. Rizzo, A. Caracausi, R. Favara, M. Martelli, A. Paonita, M. Paternoster, P. M. Nuccio, A. Rosciglione, New insights into magma dynamics during last two eruptions of Mount Etna as inferred by geochemical monitoring from 2002 to 2005. *Geochem. Geophys. Geosyst.* **7**, Q06008 (2006).
61. A. Paonita, Long-range correlation and nonlinearity in geochemical time series of gas discharges from Mt. Etna, and changes with 2001 and 2002–2003 eruptions. *Nonlinear Processes Geophys.* **17**, 733–751 (2010).
62. S. Gurrieri, M. Valenza, Gas transport in natural porous mediums: A method for measuring CO_2 flows from the ground in volcanic and geothermal areas. *Rend. Soc. Ital. Mineral. Petrol.* **43**, 1151–1158 (1988).
63. P. Francis, M. R. Burton, C. Oppenheimer, Remote measurements of volcanic gas compositions by solar occultation spectroscopy. *Nature* **396**, 567–570 (1998).
64. G. G. Salerno, M. R. Burton, C. Oppenheimer, T. Caltabiano, V. I. Tsanev, N. Bruno, Novel retrieval of volcanic SO2 abundance from ultraviolet spectra. *J. Volcanol. Geotherm. Res.* **181**, 141–153 (2009).
65. G. G. Salerno, M. R. Burton, C. Oppenheimer, T. Caltabiano, D. Randazzo, N. Bruno, V. Longo, Three-years of SO_2 flux measurements of Mt. Etna using an automated UV scanner array: Comparison with conventional traverses and uncertainties in flux retrieval. *J. Volcanol. Geotherm. Res.* **183**, 76–83 (2009).
66. G. Tamburello, Ratiocalc: Software for processing data from multicomponent volcanic gas analyzers. *Comput. Geosci.* **82**, 63–67 (2015).
67. A. Aiuppa, A. Cannata, F. Cannavò, G. Di Grazia, F. Ferrari, G. Giudice, S. Gurrieri, M. Liuzzo, M. Mattia, P. Montalto, D. Patanè, G. Puglisi, Patterns in the recent 2007–2008 activity of Mount Etna volcano investigated by integrated geophysical and geochemical observations. *Geochem. Geophys. Geosyst.* **11**, Q09008 (2010).
68. H. Shinohara, A. Aiuppa, G. Giudice, S. Gurrieri, M. Liuzzo, Variation of H_2O/CO_2 and CO_2/SO_2 ratios of volcanic gases discharged by continuous degassing of Mount Etna volcano, Italy. *J. Geophys. Res.* **113**, B09203 (2008).
69. A. Burgisser, M. Alletti, B. Scaillet, Simulating the behavior of volatiles belonging to the C–O–H–S system in silicate melts under magmatic conditions with the software D-Compress. *Comput. Geosci.* **79**, 1–14 (2015).

Acknowledgments: A.P. and A.C. acknowledge M. Martelli and A. Rizzo for sampling and analytical procedures in collecting peripheral gases and for useful discussions in noble gas data interpretation. G.S. and T.C. acknowledge F. Muré and R. Maugeri for technical assistance in the INGV-OE FLAME network. S. Cappuzzo and V. Francofonte are acknowledged for support on the INGV-PA EtnaGAS and Etnaplume network maintenance and M. Tantillo for analytical support in the INGV-PA noble gas isotope laboratory. Comments and suggestions by P. Wallace and an anonymous reviewer greatly improved the manuscript. **Funding:** This study has benefited from funding provided by the Italian Presidenza del Consiglio dei Ministri-Dipartimento della Protezione Civile (DPC). This paper does not necessarily represent DPC official opinion and policies. **Author contributions:** A.P., M.L., G.S., and C.F. conceived the concepts. G.S., A.L.S., T.C., and P.B. acquired and elaborated data of SO_2 plume degassing. M.L., G.Giuf., and G.Giud. acquired and elaborated data of CO_2/SO_2 ratios in plume. M.L., G.Giuf., and S.G. acquired and elaborated signals of CO_2 soil fluxes. A.P. and A.C. sampled and elaborated He isotope data and computed magma recharges by using He isotope modeling. A.P. wrote the manuscript with contributions by M.L., G.S., and C.F. All authors discussed the results and commented on the manuscript at all stages. **Competing interests:** The authors declare that they have no competing interests. **Data and materials availability:** All data needed to evaluate the conclusions in the paper are present in the paper and/or the Supplementary Materials. Complete data tables are available at http://doi.org/10.5281/zenodo.5084452.

Submitted 18 January 2021
Accepted 14 July 2021
Published 1 September 2021
10.1126/sciadv.abg6297

Citation: A. Paonita, M. Liuzzo, G. Salerno, C. Federico, P. Bonfanti, A. Caracausi, G. Giuffrida, A. La Spina, T. Caltabiano, S. Gurrieri, G. Giudice, Intense overpressurization at basaltic open-conduit volcanoes as inferred by geochemical signals: The case of the Mt. Etna December 2018 eruption. *Sci. Adv.* **7**, eabg6297 (2021).

ScienceAdvances

Intense overpressurization at basaltic open-conduit volcanoes as inferred by geochemical signals: The case of the Mt. Etna December 2018 eruption

Antonio PaonitaMarco LiuzzoGiuseppe SalernoCinzia FedericoPiero BonfantiAntonio CaracausiGiovanni GiuffridaAlessandro La SpinaTommaso CaltabianoSergio GurrieriGaetano Giudice

Sci. Adv., 7 (36), eabg6297.

Science Advances (ISSN) is published by the American Association for the Advancement of Science. 1200 New York Avenue NW, Washington, DC 20005. The title *Science Advances* is a registered trademark of AAAS.